Check for updates

AGU ADVANCING EARTH AND SPACE SCIENCES

Geophysical Research Letters

RESEARCH LETTER
10.1029/2023GL107511

Biological Production of Distinct Carbon Pools Drives Particle Export Efficiency in the Southern Ocean

Yibin Huang[1,2,3] and **Andrea J. Fassbender**[3]

[1]State Key Laboratory of Marine Environmental Science, College of Ocean and Earth Sciences, Xiamen University, Xiamen, China, [2]Cooperative Institute for Marine and Atmospheric Research, University of Hawaii at Mānoa, Honolulu, HI, USA, [3]NOAA/OAR Pacific Marine Environmental Laboratory, Seattle, WA, USA

Abstract We use observations from the Southern Ocean (SO) biogeochemical profiling float array to quantify the meridional pattern of particle export efficiency (PE_{eff}) during the austral productive season. Float estimates reveal a pronounced latitudinal gradient of PE_{eff}, which is quantitatively supported by a compilation of existing ship-based measurements. Relying on complementary float-based estimates of distinct carbon pools produced through biological activity, we find that PE_{eff} peaks near the region of maximum particulate inorganic carbon sinking flux in the polar antarctic zone, where net primary production (NPP) is the lowest. Regions characterized by intermediate NPP and low PE_{eff}, primarily in the subtropical and seasonal ice zones, are generally associated with a higher fraction of dissolved organic carbon production. Our study reveals the critical role of distinct biogenic carbon pool production in driving the latitudinal pattern of PE_{eff} in the SO.

Plain Language Summary Microbial organisms in seawater transform carbon dioxide into different types of carbon through photosynthesis and food web cycling. These carbon types include particulate and dissolved phases, with particles being more efficiently transferred out of the sunlit ocean via gravitational sinking. The ratio of sinking particulate organic carbon to total organic carbon production, commonly referred to as the particle export efficiency, is a metric used to describe how efficiently carbon moves from the surface to the deep ocean. Using observations from a large array of robots in the Southern Ocean, we find that the different types of biogenic carbon produced control the latitudinal gradient in particle export efficiency, which is highest in regions where particulate inorganic carbon export is greatest, even when photosynthetically fixed carbon is minimal. In other areas where phytoplankton carbon production is moderate but largely comprised of dissolved organic carbon, the particle export efficiency is lower.

Key Points:

- Meridional pattern of particle export efficiency (PE_{eff}) estimated from BGC-Argo aligns with ship-based observations in the Southern Ocean
- Low PE_{eff} in subtropical and ice-covered regions and high PE_{eff} in subpolar regions is linked to the biogenic carbon pools produced
- Most global models struggle to reproduce the meridional pattern of PE_{eff} in the Southern Ocean

Supporting Information:

Supporting Information may be found in the online version of this article.

Correspondence to:

Y. Huang,
yibin.huang@xmu.edu.cn

Citation:

Huang, Y., & Fassbender, A. J. (2024). Biological production of distinct carbon pools drives particle export efficiency in the Southern Ocean. *Geophysical Research Letters*, *51*, e2023GL107511. https://doi.org/10.1029/2023GL107511

Received 29 NOV 2023
Accepted 23 MAY 2024

© 2024. The Author(s).
This is an open access article under the terms of the Creative Commons Attribution License, which permits use, distribution and reproduction in any medium, provided the original work is properly cited.

1. Introduction

The biologically mediated production of carbon and its subsequent transfer into the ocean interior, known as the biological carbon pump, is a critical mechanism that sustains natural ocean carbon sequestration (Boyd et al., 2019; Siegel et al., 2022; Volk & Hoffert, 1985). Particulate organic carbon (POC) export efficiency (PE_{eff}), defined as the sinking flux of POC (F_{POC}) divided by the net primary production (NPP) (Buesseler, 1998; Henson et al., 2011), represents the fraction of photosynthetically fixed carbon exported out of the euphotic zone after food-web cycling. PE_{eff} is a critical metric for assessing the efficiency of the biological pump (Henson et al., 2019; Laws et al., 2000).

Due to the well-recognized importance of PE_{eff}, numerous studies have focused on estimating PE_{eff} using empirical models, food-web models, or numerical models (as summarized in Siegel et al. (2022)). Estimates of PE_{eff} and NPP based on remote-sensing observations have been used to estimate global ocean carbon export and its impact on air-sea carbon dioxide (CO_2) exchange (Arteaga et al., 2018; Emerson, 2014; Pittman et al., 2022; Siegel et al., 2022). However, current estimates of annual global carbon export vary widely (5–12 Pg C yr^{-1}), with the uncertainty exceeding the magnitude of annual global ocean CO_2 uptake (2–4 Pg C yr^{-1}) (Fay et al., 2021; Friedlingstein et al., 2022; Landschützer et al., 2014), challenging our ability to detect changes in the natural carbon cycle. Uncertainty in projections of the biological carbon pump magnitude and variability may arise from shortcomings in model parameterizations, the complexity of marine ecosystems, or the limited observational data sets available for model refinement.

The production of POC, dissolved organic carbon (DOC), and particulate inorganic carbon (PIC) in seawater reflects the integrated imprint of ecosystem dynamics. For example, sinking particles can be comprised of dead

19448007, 2024, 12, Downloaded from https://agupubs.onlinelibrary.wiley.com/doi/10.1029/2023GL107511, Wiley Online Library on [15/06/2024]. See the Terms and Conditions (https://onlinelibrary.wiley.com/terms-and-conditions) on Wiley Online Library for rules of use; OA articles are governed by the applicable Creative Commons License

phytoplankton, zooplankton fecal pellets, and aggregate material (i.e., marine snow) (Iversen, 2023). DOC primarily originates from phytoplankton excretion, zooplankton sloppy feeding, and bacterial activity (Moran et al., 2022). PIC formation in the open ocean is predominantly attributed to calcifying organisms such as coccolithophores and foraminifera (Sulpis et al., 2021). Consequently, community structure and interactions across trophic levels (i.e., grazing pressure on phytoplankton, the partitioning of carbon between classical and microbial food webs), as well as other factors such as phytoplankton physiology and bacterial activity, can significantly influence how carbon is partitioned between POC and other carbon pools (i.e., DOC and PIC), thereby impacting PE_{eff}.

In this study, we use NPP estimates derived from 113 seasonal cycles of biogeochemical (BGC) variables made by 63 profiling floats in combination with previous estimates of POC, DOC, and PIC export potential and the sinking fluxes of particle organic carbon (Huang et al., 2023), to quantify the meridional pattern of PE_{eff} in the Southern Ocean (SO). To evaluate the float estimates, we compile historical shipboard data sets of NPP (measured by ^{14}C incubation) as well as F_{POC} and F_{PIC} (measured by ^{234}Th-^{238}U disequilibrium). Interpreting our results in the context of biogenic PIC and DOC production provides new insight into the mechanisms driving the meridional pattern of PE_{eff} in the SO.

2. Methods

2.1. Data Sources

BGC-float data used in this study are archived at https://www.seanoe.org/data/00311/42182/. Float profiles made prior to September 2021 from floats simultaneously equipped with pH, dissolved oxygen, nitrate, and bio-optical sensors are used herein. Only floats with more than six profiles having sufficient data quality during each productive season are included to ensure adequate seasonal coverage. Following these criteria, a total of 63 BGC floats, covering 113 seasonal cycles, are included in the analysis (Figure 1, Figure S1 and Table S1 in Supporting Information S1). Float data quality control follows the procedures outlined in Maurer et al. (2021), with further details provided in Text S1 in Supporting Information S1.

2.2. Float-Based Estimates of Net Primary Production

NPP is calculated using depth-resolved float profiles of chlorophyll-fluorescence (Chl) observations and phytoplankton carbon (C_{phy}) estimates (Text S1 in Supporting Information S1) as inputs to the Carbon-based Productivity Model (CbPM; Westberry et al., 2008), following the methods of Arteaga et al. (2022) and Long, Fassbender, and Estapa (2021). Float-based NPP estimates assimilate subsurface properties directly from float measurements, circumventing the need for depth extrapolation that is required when using remotely sensed parameters to estimate NPP. NPP at a specific depth (z) can be expressed as a product of C_{phy} and growth rate (μ, Equation 1).

$$NPP\,(z) = C_{phy}\,(z) \times \mu\,(z) \tag{1}$$

μ can be parameterized as a function of photosynthetically available radiation (PAR) and the Chl:C ratio, which capture the impact of light (f(light)) and nutrient and temperature stresses (f(nut, T)) on growth rate, respectively (Equation 2):

$$\mu\,(z) = \underbrace{2}_{\mu_{max}} \times \underbrace{\left(1 - e^{-5\times PAR(Z)}\right)}_{f(light)} \times \underbrace{\frac{Chl(z){:}C_{phy}(z) - 0.0003}{\left(0.022 + 0.023 \times e^{-3\times PAR(Z)}\right) - 0.0003}}_{f(nut,T)} \tag{2}$$

where μ_{max} is the maximum theoretical growth rate in the absence of environmental stresses. When computating μ, we use the median PAR value within the mixed layer, as recommended by Westberry et al. (2008), and depth-resolved PAR values at depths below the mixed layer, under the assumption that phytoplankton acclimate to ambient light levels. We estimate PAR at each depth horizon using remotely sensed surface PAR and a depth-resolved light attenuation coefficient inferred from float-measured Chl profiles (Morel et al., 2007). We

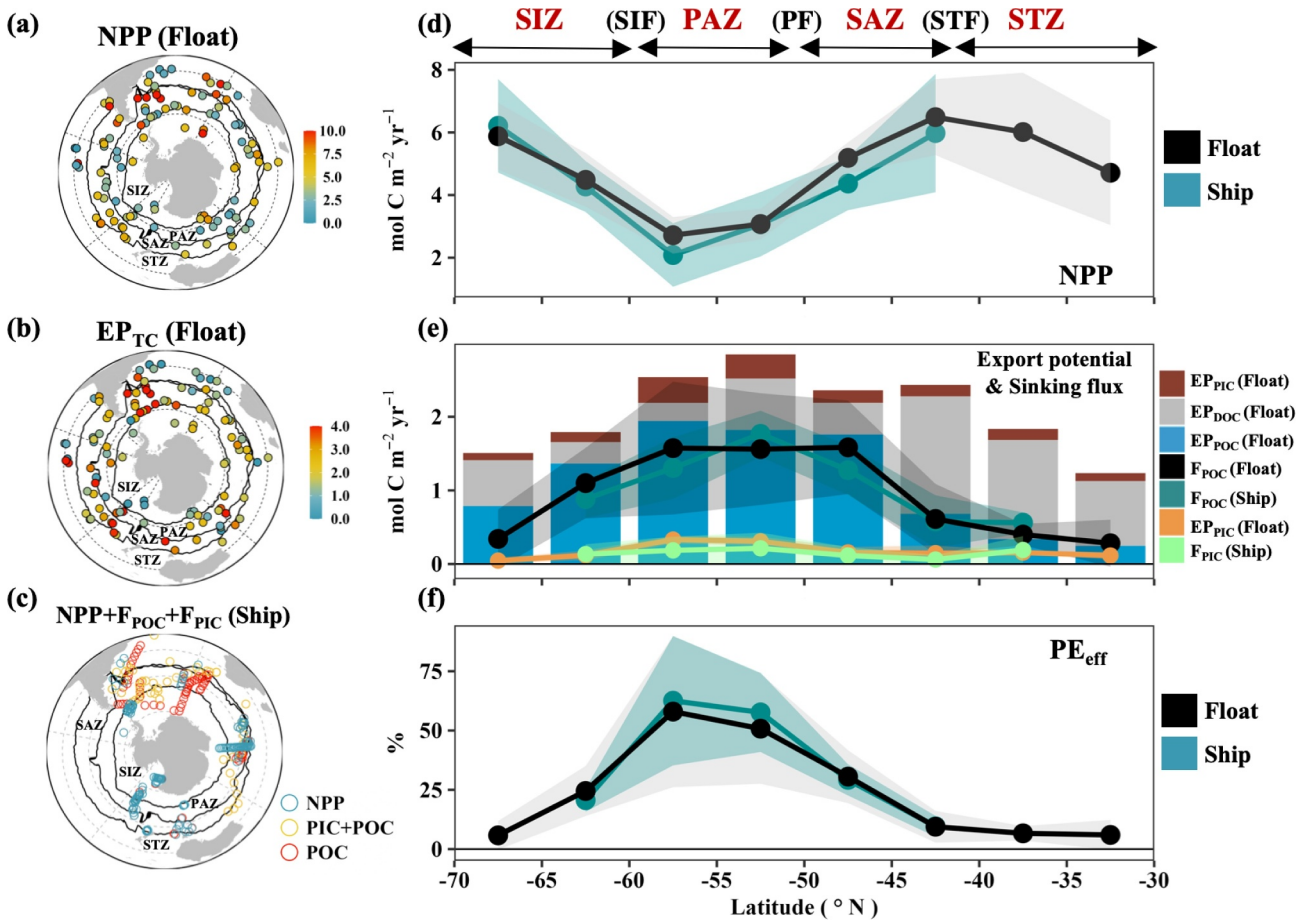

Figure 1. Float-based estimates and ship-based measurements of net primary production (NPP), export potential of distinct carbon pools, and particle sinking fluxes in the Southern Ocean during the austral productive season. Left panels show locations of (a) float-based estimates of NPP, (b) float-based estimates of total carbon export potential (EP_{TC}: biological term solved from the dissolved inorganic carbon budget representing the sum of particulate organic carbon (POC), particulate inorganic carbon (PIC), and dissolved organic carbon (DOC) export potential components) integrated over the euphotic zone, and (c) compilations of ship-based measurements of NPP and particle sinking fluxes (F_{POC} and F_{PIC}). Right panels show the meridional patterns of float- and ship-based (d) NPP, (e) export potential (EP) of distinct carbon pools (EP_{POC}, EP_{DOC}, EP_{PIC}) and particle sinking fluxes, and (f) export efficiency of sinking POC (PE_{eff} = 100% × F_{POC}/NPP). Shading in panels (d–f) reflects the propagated error. Circles in panels (a, b) show the mean float location during each productive season. Black lines in panels (a–c) show the climatological locations (mean of 2004–2014) of Southern Ocean fronts determined using an Argo-based climatology of temperature and salinity (Roemmich & Gilson, 2009). Labels above panel d indicate the approximate locations of frontal regions, with more precise locations found in left panel. STF: subtropical front; STZ: subtropical zone; SAZ: subantarctic zone; PF: polar front; PAZ: polar antarctic zone; SIF: seasonal ice zone; SIZ: sea ice zone.

then integrate the depth-resolved NPP values through the euphotic zone (Figure S2e in Supporting Information S1), defined herein as the 1% light level.

2.3. Float-Based Estimates of Export Potential and Particle Sinking Flux

Our analysis is based on existing productive period estimates of POC, DOC, and PIC export potential derived from the same float data set used to estimate NPP (Huang et al., 2023). Here we briefly summarize the methodology used to make these estimates (see Haskell et al. (2020) and Huang et al. (2023) for details). A one-dimensional mass balance model is applied to four biologically-relevant tracers (T), including: dissolved inorganic carbon (DIC), total alkalinity (TA), nitrate (NO_3^-), and suspended POC (POC_{bbp}). This allows us to isolate, as a residual, the tracer change induced by biological activity (Bio, Equation 3):

19448007, 2024, 12, Downloaded from https://agupubs.onlinelibrary.wiley.com/doi/10.1029/2023GL107511, Wiley Online Library on [15/06/2024]. See the Terms and Conditions (https://onlinelibrary.wiley.com/terms-and-conditions) on Wiley Online Library for rules of use; OA articles are governed by the applicable Creative Commons License

$$\left.\frac{\partial T_{(DIC,TA,NO_3^-,\ POC_{b_{bp}})}}{\partial t}\right|_{Bio} = \left.\frac{dT_{(DIC,TA,\ NO_3^-,POC_{b_{bp}})}}{dt}\right|_{Obs} - \left.\frac{\partial T_{(DIC)}}{\partial t}\right|_{Gas} - \left.\frac{\partial T_{(DIC,TA,\ NO_3^-,\ POC_{b_{bp}})}}{\partial t}\right|_{Phys} - \left.\frac{\partial T_{(DIC,TA,NO_3^-,\ POC_{b_{bp}})}}{\partial t}\right|_{EP} \quad (3)$$

where the subscripts on the right-hand side denote float observations (Obs), gas exchange (Gas), physical transport (Phys), and evaporation and precipitation (EP). The biological term for suspended PIC ($\left.\frac{\partial T_{(PIC)}}{\partial t}\right|_{Bio}$) is inferred from $\left.\frac{\partial T_{(\ POC_{b_{bp}})}}{\partial t}\right|_{Bio}$ using the satellite-retrieved PIC:POC ratio as a scalar.

The biological term solved from the DIC tracer budget, $\left.\frac{\partial DIC}{\partial t}\right|_{Bio}$, represents the export potential of total carbon (EP_{TC}), encompassing POC, DOC, and PIC fractions. The contributions of the total organic carbon (EP_{TOC}) and PIC (EP_{PIC}) to EP_{TC} are differentiated by relating the DIC and TA budget biological terms ($\left.\frac{\partial DIC}{\partial t}\right|_{Bio}$; $\left.\frac{\partial TA}{\partial t}\right|_{Bio}$) using well-constrained end-member nutrient ratios following the equations below (Equations 4 and 5):

$$EP_{TOC} = \frac{\left.\frac{\partial TA}{\partial t}\right|_{Bio} - \left(\frac{1}{DIC{:}TA_{PIC}} \times \left.\frac{\partial DIC}{\partial t}\right|_{Bio}\right)}{\left(\frac{1}{DIC{:}TA_{TOM}} - \frac{1}{DIC{:}TA_{PIC}}\right)} \quad (4)$$

$$EP_{PIC} = \left.\frac{\partial DIC}{\partial t}\right|_{Bio} - EP_{TOC} \quad (5)$$

where $DIC{:}TA_{TOM}$ (−117/17) and $DIC{:}TA_{PIC}$ (0.5) are the stoichiometric ratios of total organic matter and PIC production, respectively (Anderson & Sarmiento, 1994). After solving for EP_{TOC}, we combine it with $\left.\frac{\partial NO_3^-}{\partial t}\right|_{Bio}$ to differentiate the export potential of particulate organic matter (EP_{POC}) and dissolved organic matter (EP_{DOC}, Equations 6 and 7):

$$EP_{DOC} = \frac{\left.\frac{\partial NO_3^-}{\partial t}\right|_{Bio} - \left(\frac{1}{C{:}N_{POM}} \times EP_{TOC}\right)}{\frac{1}{C{:}N_{DOM}} - \frac{1}{C{:}N_{POM}}} \quad (6)$$

$$EP_{POC} = EP_{TOC} - EP_{DOC} \quad (7)$$

where $C{:}N_{DOM}$ and $C{:}N_{POM}$ are the nutrient ratios of DOM and POM production, respectively.

EP_{POC} and EP_{PIC}, as determined from the DIC chemical tracer budget, represent the total seasonal production of particles that can either be retained within the euphotic zone, leading to a seasonal increase in the upper ocean POC and PIC inventory, or lost from the euphotic zone, which we refer to as the sinking flux (F_{POC} and F_{PIC}). Thus, EP_{POC} (EP_{PIC}) may not necessarily be equivalent to F_{POC} (F_{PIC}), which is traditionally measured by ^{234}Th-^{239}U disequilibrium and sediment traps (Mouw et al., 2016). By contrast, the biological terms derived from the $POC_{b_{bp}}$ and $PIC_{b_{bp}}$ bio-optical tracer budgets ($\left.\frac{\partial POC_{b_{bp}}}{\partial t}\right|_{Bio}$ and $\left.\frac{\partial PIC}{\partial t}\right|_{Bio}$), track biologically-mediated changes in the suspended particle inventory, which reflects the total particle production (i.e., EP_{POC} and EP_{PIC}) minus the particles lost from the euphotic zone. By differencing EP_{POC} (EP_{PIC}) and $\left.\frac{\partial POC_{b_{bp}}}{\partial t}\right|_{Bio}$ ($\left.\frac{\partial PIC}{\partial t}\right|_{Bio}$), we estimate the sinking flux of particles, with an example for F_{POC} shown here (Equation 8):

$$F_{POC} = EP_{POC} - \left.\frac{\partial POC_{b_{bp}}}{\partial t}\right|_{Bio} \quad (8)$$

2.4. Ship-Based Estimates of Net Primary Production and Particle Sinking Flux

We compile historical ship-based NPP and particle sinking flux data to verify our float estimates. The archived NPP measurements typically reflect values integrated to the euphotic depth whereas compiled F_{POC} and F_{PIC} data

19448007, 2024, 12, Downloaded from https://agupubs.onlinelibrary.wiley.com/doi/10.1029/2023GL107511, Wiley Online Library on [15/06/2024]. See the Terms and Conditions (https://onlinelibrary.wiley.com/terms-and-conditions) on Wiley Online Library for rules of use; OA articles are governed by the applicable Creative Commons License

19448007, 2024, 12, Downloaded from https://agupubs.onlinelibrary.wiley.com/doi/10.1029/2023GL107511, Wiley Online Library on [15/06/2024]. See the Terms and Conditions (https://onlinelibrary.wiley.com/terms-and-conditions) on Wiley Online Library for rules of use; OA articles are governed by the applicable Creative Commons License

set are often evaluated at fixed depths other than the euphotic depth. To account for this discrepancy, we apply the Martin Curve and a global empirical attenuation factor of 0.858 (Martin et al., 1987) to interpolate the ship-based F_{POC} and F_{PIC} values to the euphotic depth at each location (Figure S2e in Supporting Information S1). As the Martin Curve is based on the vertical attenuation of F_{POC} below the euphotic zone, we exclude F_{POC} data from depths shallower than the euphotic zone before interpolation.

Ship-based F_{POC}, F_{PIC}, and euphotic-depth-integrated NPP rates are multiplied by the number of days in the productive season at each location to estimate the cumulative productive season sinking fluxes and NPP (Figure S2a in Supporting Information S1). We define the austral productive season as the period between the euphotic-zone DIC inventory maximum (ranging from September to November) and minimum (ranging from January to March of the subsequent year) (Huang et al., 2023) (Figure S2b in Supporting Information S1).

2.5. Uncertainty Estimates

We average NPP, export potential, and particle sinking flux results into 5-degree latitude bands to assess their meridional patterns. Uncertainty in the float-based estimates at each latitude band represents the error attributed to spatial and inter-annual variability (σ_S, calculated as standard error) combined with the aggregated uncertainty (σ_A) associated with each seasonal estimate derived from a Monte Carlo simulation (Table S2 in Supporting Information S1). Uncertainty in the compiled ship data set reflects σ_S.

The meridional pattern of PE_{eff} is computed as the ratio of zonal mean F_{POC} to zonal mean NPP values. This calculation approach, rather than computing PE_{eff} before averaging zonally, maximizes the amount of shipboard F_{POC} observations that can be used, as not all ship-board F_{POC} measurements are accompanied by NPP measurements. It also helps to minimize issues associated with temporal mismatches between the two measurement approaches, as the incubation-based ^{14}C-NPP measurements reflect instantaneous production while F_{POC} measurements typically reflect export several weeks prior to the sampling date (Maiti et al., 2013).

3. Results and Discussion

3.1. Meridional Patterns of NPP, Export Potential, and Particle Sinking Flux

Before interpreting our results, we first evaluate how well SO meridional patterns are represented by averages of patchy float-based estimates using 1° × 1° horizontal resolution B-SOSE model output (Verdy & Mazloff, 2017). We find excellent agreement between the meridional NPP and EP_{TOC} patterns determined by averaging B-SOSE output values (a) from grids corresponding to float locations and (b) from all grids in the SO (Figure S3 in Supporting Information S1). Thus, it is unlikely that our results are significantly biased by the float sampling distribution. Our compiled ship data set (Figure 1c) provides complementary verification of the meridional NPP and particle sinking flux patterns estimated from floats ($R^2 = 0.91$, $p < 0.01$ for NPP, $R^2 = 0.78$, $p < 0.01$ for F_{POC}).

NPP exhibits relatively high values in the subtropical zone (STZ) and seasonal ice zone (SIZ), with a minimum between these domains in the polar antarctic zone (PAZ), around 57°S (Figure 1d). The decrease in float NPP estimates between 40°S and 57°S is primarily driven by a decrease in the CbPM-modeled growth rate of phytoplankton (Equation 2, Figure S4 in Supporting Information S1). Reduced light availability (Figure S2d in Supporting Information S1) in addition to trace metal limitation (Martin, 1990; Silsbe et al., 2016; Tagliabue et al., 2017) in the subpolar region may be contributing to the depressed phytoplankton growth rates.

The mechanisms supporting elevated NPP in the STZ and SIZ appear to be distinct. In the STZ, elevated NPP is mainly driven by relatively high growth rates despite this region having the lowest biomass (Figure S4 in Supporting Information S1). A recent study by Silsbe et al. (2016), using a light-absorption-based satellite productivity model (CAFE) to back-calculate the growth rate, also found a relatively high growth rate in the subtropical ocean when compared with high-latitude regions. While it is noteworthy that estimated growth rates are higher in the subtropical regions (~0.6 $days^{-1}$) than in the subpolar regions (~0.2 $days^{-1}$), when compared to growth rates near the equator or in coastal regions (~1.2–1.5 $days^{-1}$) (Westberry et al., 2008), it is clear that these rates are still low in a broader ocean context. Relatively high growth rates in the subtropical ocean are primarily fueled by ample light availability (Figure S2d in Supporting Information S1). Additionally, the low nutrient half-saturation constants of *Prochlorococcus* and *Synechococcus* (the dominant phytoplankton species in the STZ) enable high growth rates in nutrient-depleted areas (Biller et al., 2015; Moore et al., 1995). Despite having high growth rates in the subtropical ocean, phytoplankton struggle to efficiently accumulate cell biomass. Instead, a significant

19448007, 2024, 12, Downloaded from https://agupubs.onlinelibrary.wiley.com/doi/10.1029/2023GL107511, Wiley Online Library on [15/06/2024]. See the Terms and Conditions (https://onlinelibrary.wiley.com/terms-and-conditions) on Wiley Online Library for rules of use; OA articles are governed by the applicable Creative Commons License

fraction of photosynthetically-fixed carbon is released into the ambient water as DOC, serving as an adaptive mechanism to mitigate photochemical damage (Carlson & Hansell, 2015). High grazing pressure in the oligotrophic ocean also likely contributes to maintaining the low biomass levels (Chen et al., 2013).

In the SIZ, elevated NPP results from high biomass and intermediate growth rates (Figure S4 in Supporting Information S1). Growth rates are higher in the SIZ than the adjacent PAZ due to greater light intensity, which is caused by shallower mixed layers and the polar day effect during the productive season (Figures S2d and S2e in Supporting Information S1). Additionally, sea ice melting may inject dissolved iron into the seawater, reducing iron limitation and promoting phytoplankton growth (Laufkötter et al., 2018).

Float estimates of total carbon export potential (Figure 1e) exhibit high values predominantly in the SAZ and PAZ where POC accounts for >70% of the signal. In the SIZ and STZ, where export potential is intermediate, DOC accounts for a considerable fraction of the total carbon export potential, exceeding 75% in the STZ. The maximum PIC export potential is found in PAZ. Most of the POC and PIC produced during the growing season is lost via sinking during the growing season (Figure S5 in Supporting Information S1); therefore, F_{PIC} and F_{POC} closely track the patterns of EP_{PIC} and EP_{POC}, respectively (Figure 1e).

3.2. Relationships Between Particle Export Efficiency and Carbon Pool Production

PE_{eff} peaks in the PAZ, reaching up to ~60% where NPP reaches its minimum, and decreases to around 10% in STZ and SIZ (Figure 1f). Like prior investigators (Britten et al., 2017; Laurenceau-Cornec et al., 2015; Maiti et al., 2013), we find that PE_{eff} is inversely correlated with NPP across the SO ($R^2 = 0.85$, $p < 0.05$, Figure 2a), with elevated PE_{eff} values in the PAZ and SAZ where NPP is low. This relationship could simply be due to self-correlation of NPP, since NPP is the denominator in the PE_{eff} calculation (Kenney, 1982). However, we also find an inverse relationship between NPP and F_{POC} ($R^2 = 0.50$, $p < 0.05$, Figure 2b), which suggests that the latitudinal PE_{eff} pattern is indeed caused by an inverse relationship between phytoplankton carbon fixation and POC export. Additionally, PE_{eff} increases with decreasing SST in waters >2°C (Figure 2c), aligning with prior studies (Britten et al., 2017; Maiti et al., 2013). The elevated DOC fraction in waters colder than 2°C (Figure 2c) helps to explain the seeming reversal in temperature sensitivity of PE_{eff} near the pole.

Regions with relatively high NPP and low PE_{eff}, most notably the SIZ, STZ, and northern part of the SAZ, exhibit an outsized DOC contribution to the total organic carbon export potential (>40%; bar plot in Figure 2). The elevated fraction of DOC export potential in low-latitude regions results from the combined effects of nutrient limitation and high light intensity (Huang et al., 2023). In addition to phytoplankton releasing excess fixed carbon as DOC to mitigate photochemical damage in high light conditions (Carlson & Hansell, 2015), nutrient limitation in the STZ hinders the bacterial degradation of DOC leading to a larger seasonal accumulation of DOC in the euphotic zone (Huang et al., 2019; Liu et al., 2014). For the SIZ, elevated light levels caused by shallow mixed layers and long polar days during summer (Figure S1d in Supporting Information S1), may be driving the elevated DOC contribution to total carbon production (DeVries & Deutsch, 2014).

PE_{eff} is negatively correlated with the fraction of total export potential attributed to DOC (Figure 2d, $R^2 = 0.62$, $p < 0.01$), suggesting a central role of DOC production in shaping the large-scale pattern of PE_{eff} in the SO. This finding contrasts with the study of Moigne et al. (2016) who propose a negligible impact of DOC production in modulating the PE_{eff}. However, Moigne et al. (2016) estimate biological DOC export by taking the product of diapycnal diffusivity (Kz) and the vertical DOC gradient, which represents the downward transport of DOC through diapycnal diffusion rather than the seasonal biological production of DOC. During the austral growth season when the water is stratified, diapycnal diffusion of DOC is relatively weak. Most biologically produced DOC will either accumulate in the upper layer, thereby elevating the upper ocean DOC inventory, or be respired, converting back to DIC. By misattributing the physically-mediated downward transport of DOC to biological production, Moigne et al. (2016) may underestimate the role of biological DOC production in driving PE_{eff}.

PE_{eff} is positively correlated with F_{PIC} (Figure 2e, $R^2 = 0.81$, $p < 0.01$), with both reaching maximum values in the PAZ where NPP is the lowest (Figures 1 and 2). F_{PIC} production is associated with calcifying plankton groups (i.e., coccolithophores), which are thought to act as ballast material that enhances PE_{eff} (Klaas & Archer, 2002). This hypothesis is reinforced by a strong positive relationship between F_{PIC} and PE_{eff} observed from upper ocean discrete samples during a prior field study in the SO (Balch et al., 2016). It is also worth mentioning that the PAZ is characterized by a strong meridional silicate (Si) gradient (Figure S2g in Supporting Information S1) that

19448007, 2024, 12, Downloaded from https://agupubs.onlinelibrary.wiley.com/doi/10.1029/2023GL107511, Wiley Online Library on [15/06/2024]. See the Terms and Conditions (https://onlinelibrary.wiley.com/terms-and-conditions) on Wiley Online Library for rules of use; OA articles are governed by the applicable Creative Commons License

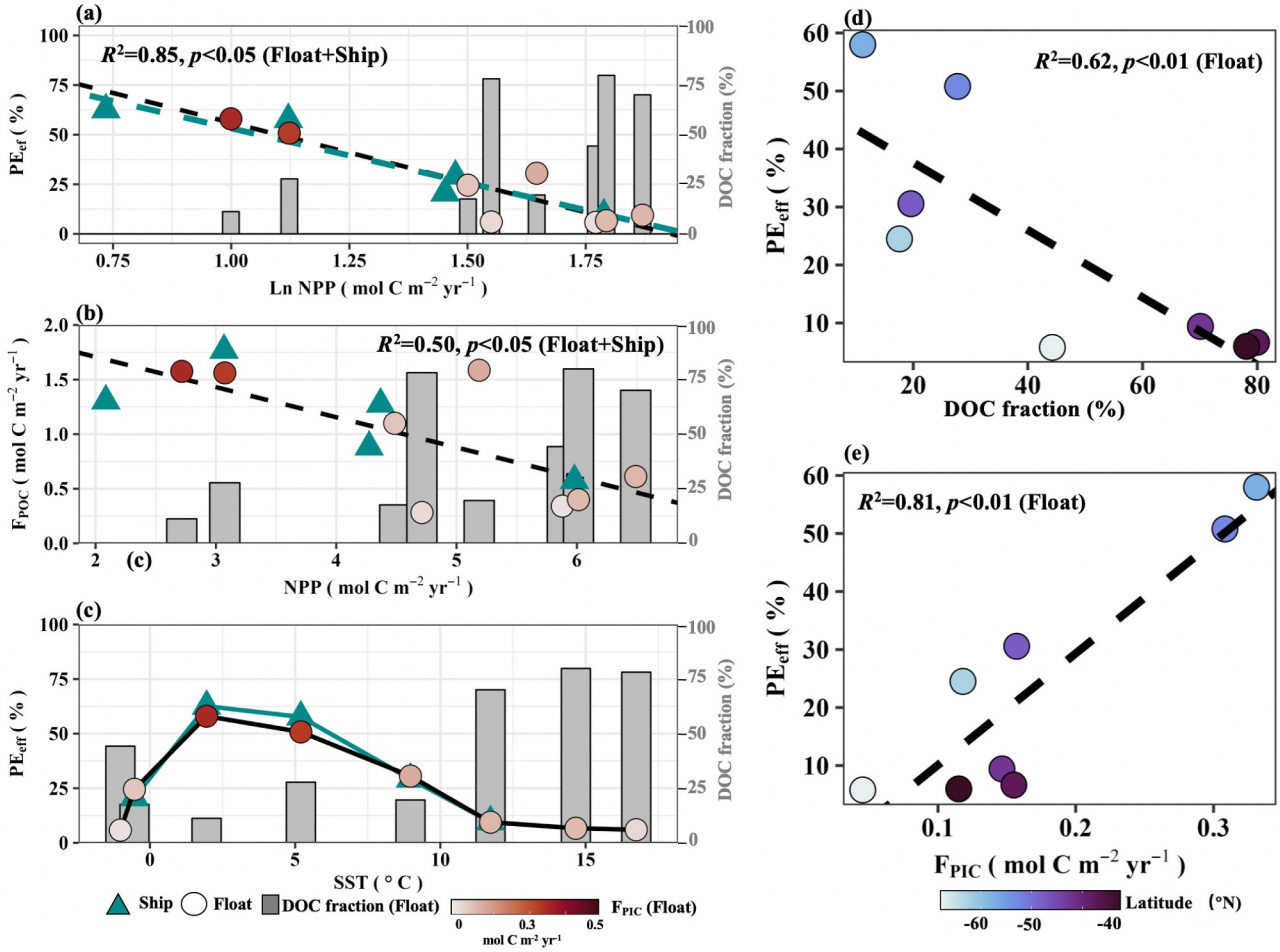

Figure 2. Relationships between (a) particulate organic carbon (POC) export efficiency (PE_{eff}) and net primary production (NPP), (b) sinking flux of POC (F_{POC}) and NPP, and (c) PE_{eff} and sea surface temperature (SST), with the fractional contribution of dissolved organic carbon (DOC) to the total carbon export potential (from floats) shown with gray bars and the sinking flux of particulate inorganic carbon (F_{PIC}; from floats) shown with red shading. Relationships between PE_{eff} and (d) the fractional contribution of DOC to the total carbon export potential and (e) F_{PIC}, respectively.

reflects thriving diatom production that consumes Si equatorward of the upwelled source waters (Sarmiento et al., 2004). Diatoms are thought to disproportionately enhance particle transfer efficiency due to their high density and large size (Armstrong et al., 2001; Boyd & Newton, 1995); however, this paradigm is challenged by some recent studies, which have found that the highest carbon fluxes are not always associated with an increase in biomineral content (Henson et al., 2012; Lam et al., 2011). Other mechanisms, such as elevated zooplankton activity that repackages phytoplankton into aggregates and fecal pellets, are also invoked to explain higher PE_{eff} values in the subpolar SO (Laurenceau-Cornec et al., 2015; Rosengard et al., 2015). A comprehensive study integrating phytoplankton community structure, trophic interactions, and sinking particle composition is needed to confirm the mechanisms driving elevated PE_{eff} in subpolar regions.

3.3. Comparison of PE_{eff} Estimates From Float Observation and Models

To evaluate our results in the context of widely used model estimates of PE_{eff} (summarized in Table S3 in Supporting Information S1), we carefully consider how each model estimate is derived. The observationally constrained empirical models are constructed using either global or SO training and validation data sets and often consider different combinations of carbon pools contributing to export. For example, the export efficiency models developed by Britten et al. (2017), Arteaga et al. (2018), and Henson et al. (2011) are trained on F_{POC} data sets, whereas the model developed by Laws et al. (2000) is trained using ^{15}N-labeled nitrate uptake to account for both POC and DOC export (e.g., EP_{TOC}; Figure 2e). The models developed by Dunne et al. (2005) and Laws

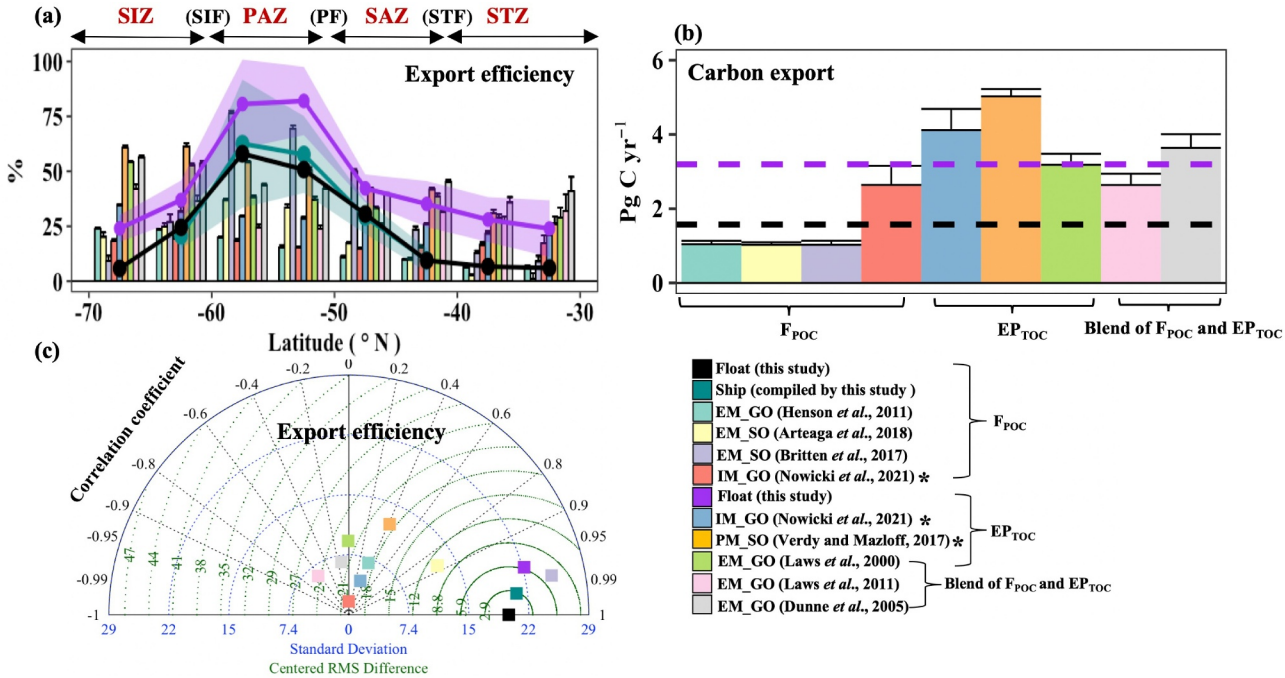

Figure 3. (a) Meridional pattern of carbon export efficiency, (b) area-weighted cumulative carbon export from the surface to the base of the euphotic zone over the Southern Ocean productive season, and (c) a Taylor diagram where all panels include data from field observations (float and ship) and models (EM: empirical model; PM: process-based model; IM: inverse model). Labels above panel a indicate the approximate locations of frontal regions, with more precise locations found in Figure 1. The vertical lines and shading in panels (a, b) represent propagated uncertainties. Carbon export estimates labeled with asterisks in the legend are obtained directly from model output while the other estimates are computed as float net primary production multiplied by carbon export efficiency. The legend indicates which carbon pools are included in each carbon export efficiency estimate (F_{POC}: particulate organic carbon; EP_{TOC}: total organic carbon) as well as the coverage of training/validation data used to develop the model (SO: Southern Ocean; GO: global ocean). RMS Difference: root mean standard difference.

et al. (2011) rely on combined data sets of F_{POC} and new production, resulting in a complex export efficiency estimate that reflects something in between the particulate and total organic carbon contributions. The B-SOSE process-based numerical model of Verdy and Mazloff (2017) provides output for the total organic carbon export efficiency, while the global inverse model used by Nowicki et al. (2022b) provides output for particulate and total organic carbon export efficiency. For comparison purposes, we include float-based estimates of both particulate (PE_{eff}) and total organic carbon export efficiency ($TOC_{eff} = 100\% \times EP_{TOC}/NPP$).

The empirical (Arteaga et al., 2018; Britten et al., 2017) and numerical (B-SOSE; Verdy and Mazloff (2017)) models trained on SO data sets outperform the models trained on global data sets (Figures 3a and 3c and Figure S6 in Supporting Information S1). The SO models tend to capture elevated PE_{eff} in the PAZ, with correlation coefficients between these estimates and the float (and ship) estimates falling within the range of 0.4 and 0.9. The best-performing model is the one developed by Britten et al. (2017) that incorporates Si concentrations to account for potential diatom ballast effects. In contrast, the globally trained models struggle to reproduce the patterns of TOC_{eff} and PE_{eff}, with correlation coefficients ranging from −0.6 to 0.3 (Figures 3a and 3c).

Our float-based estimates of area-weighted cumulative F_{POC} and EP_{TOC} during the SO productive season are 1.57 ± 0.53 Pg C yr^{-1} and 3.19 ± 0.67 Pg C yr^{-1}, respectively (Figure 3b). The models predict values ranging from 1.1 Pg C yr^{-1} to 5.1 Pg C yr^{-1} (Figure 3b); a range larger than the annual SO air-sea CO_2 flux magnitude (0.4–1.2 Pg C yr^{-1}) (Bushinsky et al., 2019; Gruber et al., 2019; Huang et al., 2023; Long, Stephens, et al., 2021). A recent study by Huang et al. (2023) underscores the importance of the biological carbon pump in maintaining the SO carbon sink by finding that a ∼30% decline in biological production could reverse the sign of the annual SO air-sea CO_2 flux, making it a carbon source to the atmosphere. Uncertainty associated with the suite of models commonly used to quantify the global biological carbon pump magnitude makes it difficult to confidently assess the role of biology in governing inter-annual variability in the global air-sea CO_2 flux.

19448007, 2024, 12, Downloaded from https://agupubs.onlinelibrary.wiley.com/doi/10.1029/2023GL107511, Wiley Online Library on [15/06/2024]. See the Terms and Conditions (https://onlinelibrary.wiley.com/terms-and-conditions) on Wiley Online Library for rules of use; OA articles are governed by the applicable Creative Commons License

19448007, 2024, 12, Downloaded from https://agupubs.onlinelibrary.wiley.com/doi/10.1029/2023GL107511, Wiley Online Library on [15/06/2024]. See the Terms and Conditions (https://onlinelibrary.wiley.com/terms-and-conditions) on Wiley Online Library for rules of use; OA articles are governed by the applicable Creative Commons License

4. Conclusions

Our study demonstrates how autonomous platforms can be used to estimate and interpret large-scale patterns of PE_{eff} in the SO. The float-based estimates of PE_{eff} align with traditional ship-based observations, and estimates from both platforms indicate an inverse relationship between NPP and F_{POC}. This causes PE_{eff} to be elevated in the subpolar region where NPP is lowest and to be depressed in the subtropical and seasonal ice-covered zones where NPP is intermediate. This relationship appears to be driven by the types of biogenic carbon produced during NPP, as PE_{eff} values are negatively correlated with the fraction of productivity attributed to dissolved organic carbon. We also find a positive correlation between PE_{eff} and the PIC sinking flux, suggesting potential export enhancement by ballast material.

Our study focuses on the SO productive season because accurately estimating carbon export during winter remains a challenge due to large errors in estimating turbulent vertical transport in upper ocean tracer budgets. Environmental perturbations and food-web dynamics in the fall and winter seasons may differ significantly from those in the stratified seasons, which could result in different relationships between PE_{eff} and carbon pool production. Extending our analysis to the entire year would provide a more complete understanding of SO PE_{eff}; requiring advancements in upper ocean diffusivity estimation. Our findings highlight substantial limitations of globally trained models that are commonly used to predict SO PE_{eff}. More data are required to improve the training and validation of global and regional PE_{eff} (and export) models, which could be achieved through a globally sustained BGC Argo array.

Conflict of Interest

The authors declare no conflict of interests.

Data Availability Statement

The float and ship-based estimates of zonal mean biologically-mediated carbon fluxes are provided in Tables S4 and S5 in Supporting Information S1, and available at Y. Huang (2024). BGC-float data used in the analysis are archived at https://www.seanoe.org/data/00311/42182/. Satellite-retrieved 8-day average PAR data at a spatial resolution of 0.083° are used to calculate NPP and are accessible on the NASA Ocean Color website (https://oceandata.sci.gsfc.nasa.gov/directdataaccess/Level-4%20Mapped/Aqua-MODIS). The ship-based NPP data set includes measurements archived on the Oregon State University Ocean Productivity website (https://sites.science.oregonstate.edu/ocean.productivity/data/field/c14/oppwgnew.txt); measurements compiled by Marra et al. (2020) (https://www.bco-dmo.org/dataset/814803), Mattei and Scardi (2021a, 2021b) (https://doi.org/10.1594/PANGAEA.932417), and Maiti et al. (2013) (extracted from their supporting information); and samples from the Atlantic Meridional Transect cruises (https://www.amt-uk.org/Data, data obtained via submitting the data request form). The shipboard F_{POC} and F_{PIC} data sets consist of those from Henson et al. (2019) (extracted from their supporting information), Rosengard et al. (2015) (extracted from Table 2 of their manuscript), and Moigne et al. (2016) (extracted from their supporting information). The output of data-assimilation global inverse model (Nowicki et al., 2022a) and a data-constrained SO ocean circulation model with embedded biogeochemical components (B-SOSE) (Verdy & Mazloff, 2017) are obtained from obtained from https://doi.org/10.6084/m9.figshare.19074521.v2 and http://sose.ucsd.edu, respectively.

Acknowledgments
We are thankful to the Southern Ocean Carbon and Climate Observations and Modeling program (SOCCOM) for float production, deployment, data quality control, and access to near real-time data. We thank Jacki Long (Monterey Bay Aquarium Research Institution) for the assistance with float estimated net primary production. Our analysis benefit from expert input provided by Adam Stoer (Dalhousie University), Dr. Marin Cornec (University of Washington), and Dr. Hannah Joy-Warren (University of Washington). Y.H. and this work was supported by a U.S. National Science Foundation (NSF) award to A.J.F. (2032754), the China NSF (42130401). A.J.F.'s was supported by NOAA PMEL. This is PMEL Contribution No. 5540.

References

Anderson, L. A., & Sarmiento, J. L. (1994). Redfield ratios of remineralization determined by nutrient data analysis. *Global Biogeochemical Cycles*, *8*(1), 65–80. https://doi.org/10.1029/93gb03318

Armstrong, R. A., Lee, C., Hedges, J. I., Honjo, S., & Wakeham, S. G. (2001). A new, mechanistic model for organic carbon fluxes in the ocean based on the quantitative association of POC with ballast minerals. *Deep Sea Research Part II: Topical Studies in Oceanography*, *49*(1), 219–236. https://doi.org/10.1016/S0967-0645(01)00101-1

Arteaga, L., Haëntjens, N., Boss, E., Johnson, K. S., & Sarmiento, J. L. (2018). Assessment of export efficiency equations in the Southern Ocean applied to satellite-based net primary production. *Journal of Geophysical Research: Oceans*, *123*(4), 2945–2964. https://doi.org/10.1002/2018jc013787

Arteaga, L. A., Behrenfeld, M. J., Boss, E., & Westberry, T. K. (2022). Vertical structure in phytoplankton growth and productivity inferred from biogeochemical-Argo floats and the Carbon-Based Productivity Model. *Global Biogeochemical Cycles*, *36*(8). https://doi.org/10.1029/2022gb007389

Balch, W. M., Bates, N. R., Lam, P. J., Twining, B. S., Rosengard, S. Z., Bowler, B. C., et al. (2016). Factors regulating the great calcite belt in the Southern Ocean and its biogeochemical significance. *Global Biogeochemical Cycles*, *30*(8), 1124–1144. https://doi.org/10.1002/2016gb005414

Biller, S. J., Berube, P. M., Lindell, D., & Chisholm, S. W. (2015). *Prochlorococcus*: The structure and function of collective diversity. *Nature Reviews Microbiology*, *13*(1), 13–27. https://doi.org/10.1038/nrmicro3378

Boyd, P., & Newton, P. (1995). Evidence of the potential influence of planktonic community structure on the interannual variability of particulate organic carbon flux. *Deep Sea Research Part I: Oceanographic Research Papers*, *42*(5), 619–639. https://doi.org/10.1016/0967-0637(95)00017-Z

Boyd, P. W., Claustre, H., Levy, M., Siegel, D. A., & Weber, T. (2019). Multi-faceted particle pumps drive carbon sequestration in the ocean. *Nature*, *568*(7752), 327–335. https://doi.org/10.1038/s41586-019-1098-2

Britten, G. L., Wakamatsu, L., & Primeau, F. W. (2017). The temperature-ballast hypothesis explains carbon export efficiency observations in the Southern Ocean. *Geophysical Research Letters*, *44*(4), 1831–1838. https://doi.org/10.1002/2016gl072378

Buesseler, K. O. (1998). The decoupling of production and particulate export in the surface ocean. *Global Biogeochemical Cycles*, *12*(2), 297–310. https://doi.org/10.1029/97GB03366

Bushinsky, S. M., Landschutzer, P., Rodenbeck, C., Gray, A. R., Baker, D., Mazloff, M. R., et al. (2019). Reassessing Southern Ocean air-Sea CO_2 flux estimates with the addition of biogeochemical float observations. *Global Biogeochemical Cycles*, *33*(11), 1370–1388. https://doi.org/10.1029/2019GB006176

Carlson, C. A., & Hansell, D. A. (2015). *DOM sources, sinks, reactivity, and budgets, Biogeochemistry of marine dissolved organic matter* (pp. 65–126). Elsevier.

Chen, B., Zheng, L., Huang, B., Song, S., & Liu, H. (2013). Seasonal and spatial comparisons of phytoplankton growth and mortality rates due to microzooplankton grazing in the northern South China Sea. *Biogeosciences*, *10*(4), 2775–2785. https://doi.org/10.5194/bg-10-2775-2013

DeVries, T., & Deutsch, C. (2014). Large-scale variations in the stoichiometry of marine organic matter respiration. *Nature Geoscience*, *7*(12), 890–894. https://doi.org/10.1038/ngeo2300

Dunne, J. P., Armstrong, R. A., Gnanadesikan, A., & Sarmiento, J. L. (2005). Empirical and mechanistic models for the particle export ratio. *Global Biogeochemical Cycles*, *19*(4). https://doi.org/10.1029/2004gb002390

Emerson, S. (2014). Annual net community production and the biological carbon flux in the ocean. *Global Biogeochemical Cycles*, *28*(1), 14–28. https://doi.org/10.1002/2013gb004680

Fay, A. R., Gregor, L., Landschützer, P., McKinley, G. A., Gruber, N., Gehlen, M., et al. (2021). SeaFlux: Harmonization of air–sea CO_2 fluxes from surface pCO_2 data products using a standardized approach. *Earth System Science Data*, *13*(10), 4693–4710. https://doi.org/10.5194/essd-13-4693-2021

Friedlingstein, P., O'Sullivan, M., Jones, M. W., Andrew, R. M., Gregor, L., Hauck, J., et al. (2022). Global carbon budget 2022. *Earth System Science Data*, *14*(11), 4811–4900. https://doi.org/10.5194/essd-14-4811-2022

Gruber, N., Landschutzer, P., & Lovenduski, N. S. (2019). The variable Southern Ocean carbon sink. *Annual Review of Marine Science*, *11*(1), 159–186. https://doi.org/10.1146/annurev-marine-121916-063407

Haskell, W. Z. II., Fassbender, A. J., Long, J. S., & Plant, J. N. (2020). Annual net community production of particulate and dissolved organic carbon from a decade of biogeochemical profiling float observations in the Northeast Pacific. *Global Biogeochemical Cycles*, *34*(10), e2020GB006599. https://doi.org/10.1029/2020GB006599

Henson, S., Le Moigne, F., & Giering, S. (2019). Drivers of carbon export efficiency in the global ocean. *Global Biogeochemical Cycles*, *33*(7), 891–903. https://doi.org/10.1029/2018GB006158

Henson, S. A., Sanders, R., & Madsen, E. (2012). Global patterns in efficiency of particulate organic carbon export and transfer to the deep ocean. *Global Biogeochemical Cycles*, *26*(1). https://doi.org/10.1029/2011gb004099

Henson, S. A., Sanders, R., Madsen, E., Morris, P. J., Le Moigne, F., & Quartly, G. D. (2011). A reduced estimate of the strength of the ocean's biological carbon pump. *Geophysical Research Letters*, *38*(4), L04606. https://doi.org/10.1029/2011gl046735

Huang, Y. (2024). Zonal mean of primary production and carbon export in the Southern Ocean (Huang and Fassbender, 2023, Geophysical Research Letters) [Dataset]. *Geophysical Research Letters. Zenodo*. https://doi.org/10.5281/zenodo.11469394

Huang, Y., Fassbender, A. J., & Bushinsky, S. M. (2023). Biogenic carbon pool production maintains the Southern Ocean carbon sink. *Proceedings of the National Academy of Sciences*, *120*(18), e2217909120. https://doi.org/10.1073/pnas.2217909120

Huang, Y. B., Laws, E., Chen, B. Z., & Huang, B. (2019). Stimulation of heterotrophic and autotrophic metabolism in the mixing zone of the Kuroshio current and northern South China sea: Implications for export production. *Journal of Geophysical Research-Biogeosciences*, *124*(9), 2645–2661. https://doi.org/10.1029/2018jg004833

Iversen, M. H. (2023). Carbon export in the ocean: A biologist's perspective. *Annual Review of Marine Science*, *15*(1), 357–381. https://doi.org/10.1146/annurev-marine-032122-035153

Kenney, B. C. (1982). Beware of spurious self-correlations. *Water Resources Research*, *18*(4), 1041–1048. https://doi.org/10.1029/WR018i004p01041

Klaas, C., & Archer, D. E. (2002). Association of sinking organic matter with various types of mineral ballast in the deep sea: Implications for the rain ratio. *Global Biogeochemical Cycles*, *16*(4), 1116. https://doi.org/10.1029/2001gb001765

Lam, P. J., Doney, S. C., & Bishop, J. K. B. (2011). The dynamic ocean biological pump: Insights from a global compilation of particulate organic carbon, $CaCO_3$, and opal concentration profiles from the mesopelagic. *Global Biogeochemical Cycles*, *25*(3). https://doi.org/10.1029/2010gb003868

Landschützer, P., Gruber, N., Bakker, D. C. E., & Schuster, U. (2014). Recent variability of the global ocean carbon sink. *Global Biogeochemical Cycles*, *28*(9), 927–949. https://doi.org/10.1002/2014gb004853

Laufkötter, C., Stern, A. A., John, J. G., Stock, C. A., & Dunne, J. P. (2018). Glacial iron sources stimulate the Southern Ocean carbon cycle. *Geophysical Research Letters*, *45*(24), 13377–313385. https://doi.org/10.1029/2018GL079797

Laurenceau-Cornec, E. C., Trull, T. W., Davies, D. M., Bray, S. G., Doran, J., Planchon, F., et al. (2015). The relative importance of phytoplankton aggregates and zooplankton fecal pellets to carbon export: Insights from free-drifting sediment trap deployments in naturally iron-fertilised waters near the Kerguelen plateau. *Biogeosciences*, *12*(4), 1007–1027. https://doi.org/10.5194/bg-12-1007-2015

Laws, E. A., D'Sa, E., & Naik, P. (2011). Simple equations to estimate ratios of new or export production to total production from satellite-derived estimates of sea surface temperature and primary production. *Limnology and Oceanography: Methods*, *9*(12), 593–601. https://doi.org/10.4319/lom.2011.9.593

Laws, E. A., Falkowski, P. G., Smith, W. O., Ducklow, H., & McCarthy, J. J. (2000). Temperature effects on export production in the open ocean. *Global Biogeochemical Cycles*, *14*(4), 1231–1246. https://doi.org/10.1029/1999gb001229

Liu, J., Jiao, N., & Tang, K. (2014). An experimental study on the effects of nutrient enrichment on organic carbon persistence in the western Pacific oligotrophic gyre. *Biogeosciences*, *11*(18), 5115–5122. https://doi.org/10.5194/bg-11-5115-2014

19448007, 2024, 12, Downloaded from https://agupubs.onlinelibrary.wiley.com/doi/10.1029/2023GL107511, Wiley Online Library on [15/06/2024]. See the Terms and Conditions (https://onlinelibrary.wiley.com/terms-and-conditions) on Wiley Online Library for rules of use; OA articles are governed by the applicable Creative Commons License

Long, J. S., Fassbender, A. J., & Estapa, M. L. (2021a). Depth-resolved net primary production in the northeast Pacific ocean: A comparison of satellite and profiling float estimates in the context of two marine heatwaves. *Geophysical Research Letters*, *48*(19). https://doi.org/10.1029/2021gl093462

Long, M. C., Stephens, B. B., McKain, K., Sweeney, C., Keeling, R. F., Kort, E. A., et al. (2021). Strong Southern Ocean carbon uptake evident in airborne observations. *Science*, *374*(6572), 1275–1280. https://doi.org/10.1126/science.abi4355

Maiti, K., Charette, M. A., Buesseler, K. O., & Kahru, M. (2013). An inverse relationship between production and export efficiency in the Southern Ocean. *Geophysical Research Letters*, *40*(8), 1557–1561. https://doi.org/10.1002/grl.50219

Marra, J. F., Barber, R. T., Barber, E., Bidigare, R. R., Chamberlin, W. S., Goericke, R., et al. (2020). A database of ocean primary productivity from the ^{14}C method. *Limnology and Oceanography Letters*, *6*(2), 107–111. https://doi.org/10.1002/lol2.10175

Martin, J. H. (1990). Glacial-interglacial CO_2 change: The iron hypothesis. *Paleoceanography*, *5*(1), 1–13. https://doi.org/10.1029/PA005i001p00001

Martin, J. H., Knauer, G. A., Karl, D. M., & Broenkow, W. W. (1987). VERTEX: Carbon cycling in the northeast Pacific. *Deep-Sea Research Part I Oceanographic Research Papers*, *34*(2), 267–285. https://doi.org/10.1016/0198-0149(87)90086-0

Mattei, F., & Scardi, M. (2021a). Collection and analysis of a global marine phytoplankton primary-production dataset. *Earth System Science Data*, *13*(10), 4967–4985. https://doi.org/10.5194/essd-13-4967-2021

Mattei, F., & Scardi, M. (2021b). Global marine phytoplankton production dataset [Dataset]. *PANGAEA*. https://doi.org/10.1594/PANGAEA.932417

Maurer, T. L., Plant, J. N., & Johnson, K. S. (2021). Delayed-mode quality control of oxygen, nitrate, and pH data on SOCCOM biogeochemical profiling floats. *Frontiers in Marine Science*, *8*. https://doi.org/10.3389/fmars.2021.683207

Moigne, F. A. C. L., Henson, S. A., Cavan, E., Georges, C., Pabortsava, K., Achterberg, E. P., et al. (2016). What causes the inverse relationship between primary production and export efficiency in the Southern Ocean? *Geophysical Research Letters*, *43*(9), 4457–4466. https://doi.org/10.1002/2016gl068480

Moore, L. R., Goericke, R., & Chisholm, S. W. (1995). Comparative physiology of *Synechococcus* and *Prochlorococcus*: Influence of light and temperature on growth, pigments, fluorescence and absorptive properties. *Marine Ecology Progress Series*, *116*, 259–275. https://doi.org/10.3354/meps116259

Moran, M. A., Ferrer-González, F. X., Fu, H., Nowinski, B., Olofsson, M., Powers, M. A., et al. (2022). The Ocean's labile DOC supply chain. *Limnology & Oceanography*, *67*(5), 1007–1021. https://doi.org/10.1002/lno.12053

Morel, A., Huot, Y., Gentili, B., Werdell, P. J., Hooker, S. B., & Franz, B. A. (2007). Examining the consistency of products derived from various ocean color sensors in open ocean (Case 1) waters in the perspective of a multi-sensor approach. *Remote Sensing of Environment*, *111*(1), 69–88. https://doi.org/10.1016/j.rse.2007.03.012

Mouw, C. B., Barnett, A., McKinley, G. A., Gloege, L., & Pilcher, D. (2016). Global ocean particulate organic carbon flux merged with satellite parameters. *Earth System Science Data*, *8*(2), 531–541. https://doi.org/10.5194/essd-8-531-2016

Nowicki, M., DeVries, T., & Siegel, D. (2022a). Ocean biological carbon pump model output (Version 2) [Dataset]. https://doi.org/10.6084/m9.figshare.19074521.v2

Nowicki, M., DeVries, T., & Siegel, D. A. (2022b). Quantifying the carbon export and sequestration pathways of the ocean's biological carbon pump. *Global Biogeochemical Cycles*, *36*(3). https://doi.org/10.1029/2021gb007083

Pittman, N. A., Strutton, P. G., Johnson, R., Matear, R. J., & Sutton, A. J. (2022). Relationships between air-sea CO_2 flux and new production in the Equatorial Pacific. *Global Biogeochemical Cycles*, *36*(4). https://doi.org/10.1029/2021gb007121

Roemmich, D., & Gilson, J. (2009). The 2004–2008 mean and annual cycle of temperature, salinity, and steric height in the global ocean from the Argo Program. *Progress in Oceanography*, *82*(2), 81–100. https://doi.org/10.1016/j.pocean.2009.03.004

Rosengard, S. Z., Lam, P. J., Balch, W. M., Auro, M. E., Pike, S., Drapeau, D., & Bowler, B. (2015). Carbon export and transfer to depth across the Southern Ocean Great calcite Belt. *Biogeosciences*, *12*(13), 3953–3971. https://doi.org/10.5194/bg-12-3953-2015

Sarmiento, J. L., Gruber, N., Brzezinski, M. A., & Dunne, J. P. (2004). High-latitude controls of thermocline nutrients and low latitude biological productivity. *Nature*, *427*(6969), 56–60. https://doi.org/10.1038/nature02127

Siegel, D. A., DeVries, T., Cetinic, I., & Bisson, K. M. (2022). Quantifying the ocean's biological pump and its carbon cycle impacts on global scales. *Annual Review of Marine Science*, *15*(1), 329–356. https://doi.org/10.1146/annurev-marine-040722-115226

Silsbe, G. M., Behrenfeld, M. J., Halsey, K. H., Milligan, A. J., & Westberry, T. K. (2016). The CAFE model: A net production model for global ocean phytoplankton. *Global Biogeochemical Cycles*, *30*(12), 1756–1777. https://doi.org/10.1002/2016gb005521

Sulpis, O., Jeansson, E., Dinauer, A., Lauvset, S. K., & Middelburg, J. J. (2021). Calcium carbonate dissolution patterns in the ocean. *Nature Geoscience*, *14*(6), 423–428. https://doi.org/10.1038/s41561-021-00743-y

Tagliabue, A., Bowie, A. R., Boyd, P. W., Buck, K. N., Johnson, K. S., & Saito, M. A. (2017). The integral role of iron in ocean biogeochemistry. *Nature*, *543*(7643), 51–59. https://doi.org/10.1038/nature21058

Verdy, A., & Mazloff, M. R. (2017). A data assimilating model for estimating Southern Ocean biogeochemistry. *Journal of Geophysical Research: Oceans*, *122*(9), 6968–6988. https://doi.org/10.1002/2016jc012650

Volk, T., & Hoffert, M. I. (1985). Ocean carbon pumps: Analysis of relative strengths and efficiencies in ocean-driven atmospheric CO_2 changes, the carbon cycle and atmospheric CO_2: Natural variations Archean to present. https://doi.org/10.1029/GM032p0099

Westberry, T., Behrenfeld, M. J., Siegel, D. A., & Boss, E. (2008). Carbon-based primary productivity modeling with vertically resolved photoacclimation. *Global Biogeochemical Cycles*, *22*(2), 85. https://doi.org/10.1029/2007gb003078

References From the Supporting Information

Behrenfeld, M. J., Boss, E., Siegel, D. A., et al. (2005). Carbon-based ocean productivity and phytoplankton physiology from space. *Global Biogeochemical Cycles*, *19*(1), GB1006. https://doi.org/10.1029/2004GB002299

Bittig, H. C., Steinhoff, T., Claustre, H., et al. (2018). An alternative to static climatologies: Robust estimation of open ocean CO_2 variables and nutrient concentrations from T, S, and O_2 data using Bayesian Neural Networks. *Frontiers in Marine Science*, *5*. https://doi.org/10.3389/fmars.2018.00328

Boyer, T., Baranova, O., Coleman, C., et al. (2018). World Ocean Database 2018. (in preparation).

Briggs, N., Perry, M. J., Cetinić, I., et al. (2011). High-resolution observations of aggregate flux during a sub-polar North Atlantic spring bloom. *Deep Sea Research Part I: Oceanographic Research Papers*, *58*(10), 1031–1039. https://doi.org/10.1016/j.dsr.2011.07.007

Huang, Y., Fassbender, A. J., Long, J. S., et al. (2022). Partitioning the export of distinct biogenic carbon pools in the Northeast Pacific Ocean using a biogeochemical profiling float. *Global Biogeochemical Cycles*, *36*(2). https://doi.org/10.1029/2021gb007178

19448007, 2024, 12, Downloaded from https://agupubs.onlinelibrary.wiley.com/doi/10.1029/2023GL107511, Wiley Online Library on [15/06/2024]. See the Terms and Conditions (https://onlinelibrary.wiley.com/terms-and-conditions) on Wiley Online Library for rules of use; OA articles are governed by the applicable Creative Commons License

Johnson, K. S., Mazloff, M. R., Bif, M. B., et al. (2022). Carbon to nitrogen uptake ratios observed across the Southern Ocean by the SOCCOM profiling float array. *Journal of Geophysical Research: Oceans*, *127*(9). https://doi.org/10.1029/2022jc018859

Johnson, K. S., Plant, J. N., Coletti, L. J., et al. (2017). Biogeochemical sensor performance in the SOCCOM profiling float array. *Journal of Geophysical Research: Oceans*, *122*(8), 6416–6436. https://doi.org/10.1002/2017jc012838

Loisel, H., Nicolas, J.-M., Sciandra, A., et al. (2006). Spectral dependency of optical backscattering by marine particles from satellite remote sensing of the global ocean. *Journal of Geophysical Research*, *111*(C9). https://doi.org/10.1029/2005jc003367

Xing, X., Briggs, N., Boss, E., et al. (2018). Improved correction for non-photochemical quenching of in situ chlorophyll fluorescence based on a synchronous irradiance profile. *Optics Express*, *26*(19), 24734–24751. https://doi.org/10.1364/OE.26.024734

Yang, B., Fox, J., Behrenfeld, M. J., et al. (2021). In situ estimates of net primary production in the western North Atlantic with Argo profiling floats. *Journal of Geophysical Research: Biogeosciences*, *126*(2). https://doi.org/10.1029/2020jg006116

19448007, 2024, 12, Downloaded from https://agupubs.onlinelibrary.wiley.com/doi/10.1029/2023GL107511, Wiley Online Library on [15/06/2024]. See the Terms and Conditions (https://onlinelibrary.wiley.com/terms-and-conditions) on Wiley Online Library for rules of use; OA articles are governed by the applicable Creative Commons License